Imaging of Atomic Layer Deposited (ALD) Tungsten Monolayers on α-TiO_2(110) by X-ray Standing Wave Fourier Inversion

Chang-Yong Kim,*,†,‡ Jeffrey W. Elam,§ Michael J. Pellin,|| Dipak K. Goswami,† Steven T. Christensen,†,‡ Mark C. Hersam,†,‡ Peter C. Stair,‡,⊥,# and Michael J. Bedzyk†,‡,||

Department of Materials Science and Engineering, Institute for Environmental Catalysis, and Department of Chemistry, Northwestern University, Evanston, Illinois 60208, and Energy Systems, Materials Science, and Chemistry Divisions, Argonne National Laboratory, Argonne, Illinois 60439

Received: March 6, 2006; In Final Form: May 3, 2006

A single atomic layer of tungsten grown by atomic layer deposition (ALD) on a single-crystal rutile TiO_2(110) support is studied by the X-ray standing wave (XSW) technique. The surface structural and chemical properties were also examined using atomic force microscopy, X-ray photoelectron spectroscopy, and low-energy electron diffraction. The XSW measured set of *hkl* Fourier components for the W atomic distribution function are summed together to produce a model-independent 3D map of the W atoms relative to the rutile lattice. The 3D atomic image shows surface tungsten atoms equally occupying the two nonequivalent Ti sites with a slight outward displacement. This corresponds to the atop and bridge sites with respect to the underlying lattice oxygen atoms. These XSW measurements clearly show that ALD conformal layers can be highly coherent with respect to the substrate lattice.

Introduction

Ultrathin metallic or metal-oxide layers deposited onto oxide surfaces have wide applications in microelectronics, catalysis, photonics, and chemical sensing.[1−4] Continuing size reduction of devices and development of three-dimensional architectures for microelectronic circuits stimulate elaborate efforts toward effective film growth methods that can produce high aspect ratio structures.[5,6] Recent application trends in heterogeneous catalysis based on dispersion of catalysts over an artificial structure, such as anodized aluminum membrane[7,8] or three-dimensional photonic crystal with highly porous structure,[9] also promote development of conformal film deposition methods.

As a thin-film processing method, atomic layer deposition (ALD) provides outstanding control over the synthesis of supported materials due to its capacity for self-terminating conformal layer formation.[10] ALD has been used to fabricate high-*k* dielectric films[11] and tungsten contacts/plugs in the semiconductor industry[6,12−14] and to synthesize catalytic phases on porous or dispersed high surface area substrates.[15] The self-limiting nature of ALD provides a digital-control of epitaxial layers and has been used for III−V, II−VI, and nanolaminate film growth.[16]

Despite the increasing interest in ALD over the past decade, the majority of studies are focused on issues such as proper chemistry (search for precursors), growth procedure, and chemical composition of surface species. Most descriptions of the ALD process emphasize the cyclic procedure that occurs once the substrate is buried under an initiating ALD layer. However, the initial layer becomes critical as the desired film thickness approaches a few nanometers. The nucleation process of initiating the interface layer in ALD film growth needs to be understood for precise thickness control and maximum smoothness.[12,13,17]

In the field of heterogeneous catalysis, the interface between supported catalysts and oxide substrates has been suggested as the site of catalytic activity, i.e., the activity occurs at the 2D (monolayer or submonolayer) region, not at the 3D islands.[18,19] Due to its self-terminating property, ALD can prepare ultrathin catalyst layers without ever forming 3D islands and hence emphasize the interface effect without interference from a 3D island. Also, ALD can be employed to simultaneously fabricate single-crystal model systems and complex practical systems such as porous membranes and powders. The characterization of element-specific atomic-scale structure of ALD-grown systems would provide a unique opportunity to bridge the materials preparation gap between fundamental research and technical applications in heterogeneous catalysis.

The X-ray standing wave (XSW) method has been developed to study the bonding geometry of impurities in bulk[20,21] and adsorbed atoms on surfaces and at the liquid−solid interface.[22−27] The X-ray standing wave is generated in and above the surface of a single crystal by the coherent interference between the incident and Bragg diffracted X-ray beams. The XSW period matches the period of the diffraction planes. By scanning the incident angle through the arc-second wide H (=*hkl*) Bragg diffraction condition, the XSW nodal planes move inward in the $-\mathbf{H}$ direction by one-half of a d spacing (d_H). The X-ray fluorescence (XRF) modulation induced by the shift of the XSW can be analyzed by dynamic diffraction theory to directly determine the coherent fraction (f_H) and coherent position (P_H), which are the amplitude and phase, respectively, of the corresponding Hth Fourier component of the XRF-selected atom density distribution. Recently, a model-independent, element-specific direct-space imaging technique has been developed that

* cykim@northwestern.edu.
† Department of Materials Science and Engineering, Northwestern University.
‡ Institute for Environmental Catalysis, Northwestern University.
§ Energy Systems Division, Argonne National Laboratory.
|| Materials Science Division, Argonne National Laboratory.
⊥ Chemistry Division, Argonne National Laboratory.
Department of Chemistry, Northwestern University.

10.1021/jp061391s CCC: $33.50
Published on Web 06/02/2006

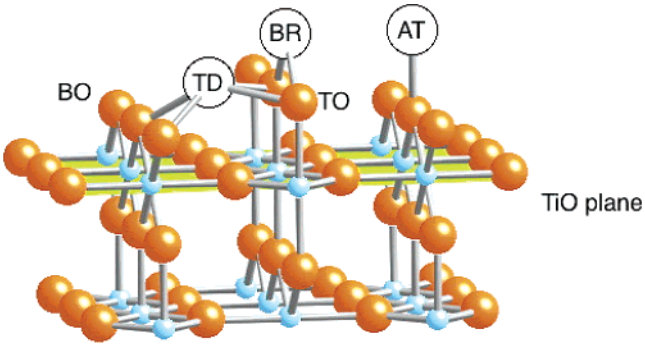

Figure 1. A ball-and-stick model of TiO_2(110) structure. The model shows one of the possible surface terminations in which two types of oxygen atoms bind to Ti cations (bridging oxygen (BO) and terminal oxygen (TO) are present). The same model represents the hydroxylated surface if the surface oxygen atoms are replaced by the hydroxyl group. Solid circles denote possible adsorption sites: atop (AT), bridge (BR), and tetradentate (TD) sites.

is based on Fourier synthesis of the atom density distribution from the XSW coherent fractions and positions.[21,24−26,28]

The W/TiO_2 system was chosen for this initial study in part because both materials have broad technological relevance and because rutile TiO_2 has been extensively studied using XSW methods.[26,29] Tungsten has been used extensively in 3D multilevel interconnections and contacts in microelectronic circuits,[30] and its oxides also have wide applications in smart windows, gas sensors, and heterogeneous catalysis.[31,32] In addition, the procedure for depositing W thin films by ALD is well-established.[14,17] Rutile α-TiO_2(110) has been used extensively as a supporting oxide substrate in practical applications and in model studies of heterogeneous catalysis.[33] The expected starting surface in air is a fully hydroxylated α-TiO_2(110) surface whose structural model[34−36] is shown in Figure 1. The surface hydroxyls are quite important because these chemical species initiate the nucleation and growth of ALD W on oxide surfaces.[13,17]

There are three different bonding configurations for oxygen atoms on this surface. The first is oxygens located in the horizontal TiO plane. The other two are oxygens located in successive planes above the TiO plane. These are the bridging oxygens (BO) that bridge between two underlying Ti atoms and terminal oxygens (TO) that occupy atop sites relative to the Ti underneath. Accordingly, the (110) surface can have three possible terminations, where the topmost layer could be the TiO plane, or the bridging oxygen (BO) layer, or the terminal oxygen (TO) layer. In ultrahigh vacuum (UHV) prepared rutile TiO_2(110) surfaces, the bridging oxygen layer has been found to be the most stable surface termination.[33] An infinite bulk crystal cleaved along a plane that lies between the BO and TO layers will produce two semi-infinite crystals both with BO termination. In the BO-terminated surface, the terminal oxygen atoms are absent, leaving one-half of the Ti atoms in the TiO plane as fivefold coordinated. However, hydroxylation of the TiO_2(110) surface fills the terminal oxygen sites with oxygen of surface hydroxyl groups.[34−37] As shown in Figure 1, high-symmetry adsorption sites on the hydroxyl-saturated TiO_2(110) surface include atop (AT), bridging (BR), and tetradentate (TD) sites. In the rutile bulk structure, Ti cations occupy octahedral sites. On the surface, the octahedral sites correspond to Ti being atop of underlying bridging oxygen and Ti bridging between two underlying terminal oxygen atoms. Atoms adsorbed at tetradentate sites (TD in Figure 1) bond to both the terminal oxygens and the bridging oxygens.

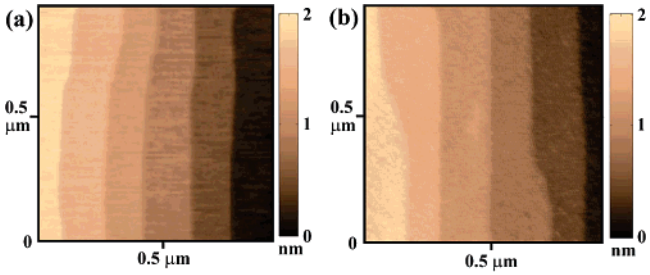

Figure 2. (a) AFM image of the TiO_2(110) surface preceding tungsten ALD. (b) AFM image of the TiO_2(110) surface following tungsten ALD. Both of these images possess broad atomically flat terraces with clearly defined step edges. The preservation of the original surface morphology and the absence of clusters following tungsten ALD suggests uniform and atomically smooth tungsten deposition.

Experimental Methods

Polished 10 × 10 × 1 mm^3 rutile (110) single crystals were obtained from Crystal GmbH. The rutile support was first annealed in air at 950 °C for 4 h, then exposed to UV radiation ($h\nu$ = 240 nm) for 5 min in air. The sample was then immersed in deionized water (resistivity > 10^{18} Ω cm^{-1}) at 90 °C for 1 h, rinsed with dilute HCl and H_2O, and then blown-dry with N_2. The substrate was further dried in the ALD reactor, using an ultrahigh-purity N_2 flow at 360 sccm at a pressure of 1 Torr for 10 min at 200 °C. The ALD reactor used in this sample preparation is described elsewhere.[38] With the sample temperature at 200 °C, the W ALD process began with 10 min exposure of the substrate to Si_2H_6 at 10 Torr, followed by 10 min exposure to WF_6 at 10 Torr. Following each exposure, the reactor was evacuated below 0.05 Torr and subsequently purged with ultrahigh-purity nitrogen for 5 min. The process of exposure to Si_2H_6, purging with nitrogen, exposure to WF_6, and finally purging with nitrogen is for the purposes of this paper the definition of one ALD cycle.

It should be noted that the exposure times utilized in this experiment are meant to be extremely long, allowing complete saturation of the surface even for a relatively unreactive single crystal. Long exposure times (particularly for Si_2H_6) have been shown to be effective in reducing nucleation times for W on SiO_2[13] and Al_2O_3 [17] surfaces. We have also confirmed the effectiveness of long exposures for ALD-grown W on ALD grown TiO_2.

The surface morphology was examined by atomic force microscopy (AFM) at various steps of the preparation. A Thermomicroscopes CP Research AFM operating in intermittent-contact mode provided the topography images of the substrates. The cantilevers used were silicon Thermomicroscopes Ultralevers with a probe tip radius of 10 nm, a spring constant of 3.2 N/m, and a resonant frequency of ∼75 kHz. AFM images were taken in ambient conditions. Image processing consisted of a third-order background subtraction to account for nonlinearity in the AFM piezo-scanner. As seen in Figure 2a, the annealed TiO_2(110) surface preceding tungsten ALD showed large atomically flat terraces separated by atomic steps. Similarly, following tungsten ALD, Figure 2b reveals that the ALD-produced surface showed no loss in step morphology or precipitate particle formation. Consequently, from the perspective of AFM, the tungsten ALD appears to have resulted in uniform and atomically smooth tungsten deposition.

X-ray photoelectron spectroscopy (XPS) and low-energy electron diffraction (LEED) measurements were performed in a UHV chamber with 1 × 10^{-10} Torr base pressure after in-air annealing. The non-monochromatic Mg Kα radiation ($h\nu$ =

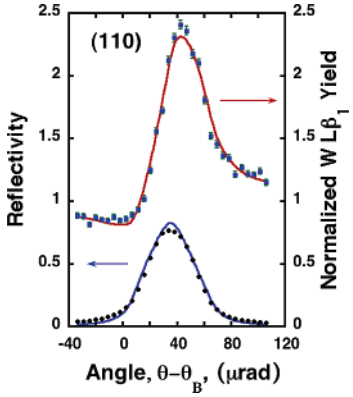

Figure 3. XSW data and theoretical fits for the TiO_2 (110) reflectivity and W Lβ_1 XRF yield as a function of incident angle. The (110) coherent position and coherent fraction determined from this fit are listed in Table 1.

1253.6 eV) and hemispherical analyzer were used as X-ray excitation source and photoelectron energy analyzer, respectively. The XPS spectrum shows existence of adventitious carbon and OH, which is typical for a sample exposed to air. Nevertheless, the LEED pattern was (1 × 1) with a slightly bright background indicating that most of the bulk-truncated, surface atomic ordering is preserved.

After the one tungsten ALD cycle, the substrate was removed from the reactor and placed on a four-circle diffractometer for XSW measurements at the Advanced Photon Source (APS) 12ID-D station. The sample was kept under a flow of dry nitrogen gas during the measurements. An incident photon energy of 13.5 keV was selected with a Si(111) monochromator and collimated further with either Si(111) or (220) channel-cut postmonochromator crystals. An energy-dispersive solid-state detector was used to collect X-ray fluorescence. The tungsten coverage was determined by comparing the W Lβ fluorescence from the sample with Pb fluorescence from an implanted standard sample with known Pb area density. One monolayer is defined as the area density of Ti atoms in the (110) TiO plane, or 10.4 atoms/nm^2. The XSW induced modulation of W Lβ fluorescence was used to determine the coherent positions, the coherent fractions, and subsequently the 3D direct-space image of W atomic distributions with respect to the rutile tetragonal primitive unit cell.

Results and Discussion

The W coverage was determined to be 0.38 ML. Figure 3 shows the (110) XSW measurement and analysis that is sensitive to the tungsten adsorption geometry along the surface normal direction. The coherent position 0.07(1) indicates that tungsten has an average adsorption height of 3.48(3) Å above the TiO plane. The set of XSW measured coherent positions and coherent fractions at the chosen set of *hkl* Bragg reflections are listed in Table 1.

The traditional XSW triangulation method could lead to tungsten lattice positions (leading to adsorption sites) after an elaborate modeling procedure.[22] However, the 3D imaging method based on Fourier synthesis of the XSW measured phase and amplitude of atom density distribution directly provides adsorption site(s) and occupation fraction(s) in a model-independent way. The imaging method is particularly useful for cases with multiple adsorption sites.[24−26] Indeed, the Fourier synthesized tungsten atom density map (Figure 4) reveals that, laterally, W occupies two symmetrically nonequivalent Ti bulklike sites that are shifted outward by 0.2 Å from the ideal bulklike Ti position.

TABLE 1: Comparison of Measured Coherent Positions (P_H) and Fractions (f_H) with Those Derived from Calculation Based on a Best-Fit Model[a]

reflection (*h k l*)	P meas	P calcd	*f* meas	*f* calcd
1 1 0	0.07 (1)	0.06	0.63 (5)	0.64
1 0 1	0.03 (1)	0.03	0.59 (4)	0.63
2 0 0	0.08 (1)	0.06	0.62 (4)	0.59
1 1 1	−0.19 (1)	−0.19	0.23 (3)	0.19
2 1 1	0.13 (1)	0.09	0.64 (8)	0.47
2 2 0	0.02 (3)	0.12	0.16 (1)	0.42
3 0 1	0.12 (1)	0.09	0.37 (2)	0.40
1 1 2	0.05 (1)	0.06	0.36 (2)	0.42
3 2 1	0.25 (2)	0.15	0.48 (7)	0.26
2 0 2	−0.03 (2)	0.06	0.40 (3)	0.38

[a] In the best-fit model, the bridge and atop sites have adsorption heights of 3.60 ± 0.08 Å and 3.28 ± 0.08 Å above the unrelaxed TiO plane, respectively.

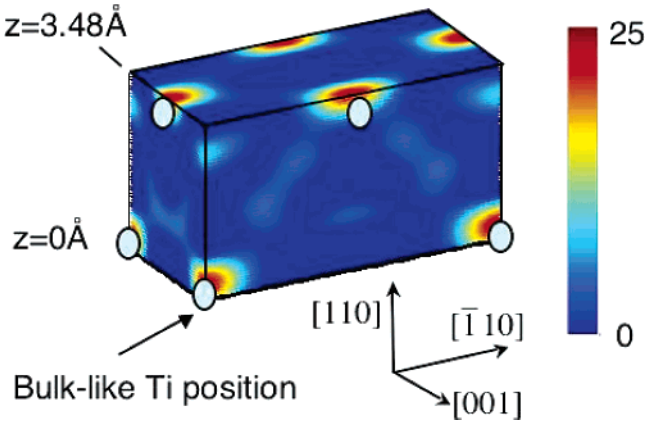

Figure 4. 3D W atom density map generated by the summation of several TiO_2 (*hkl*) XSW measured Fourier components. As a point of reference open circles denoting the ideal bulklike Ti sites are also shown at heights of 0 and 3.25 Å as expected from the ideal extension of the support above the surface.

The adsorption geometry for the tungsten atoms is further refined by a least-squares fit of the measured coherent fractions and positions to those calculated from models compatible with the model-independent 3D image. Tetradentate adsorption, which has been observed for various ions in aqueous−solid interface,[26,27] was ruled out. In our model, we partitioned the W distribution into three parts: random W, BR W, and AT W. This model can be described by five free parameters, namely, the ordered or nonrandom fraction (C), the fraction of ordered W atoms that occupy the BR-site (c_B), the two different heights for the W atoms above the TiO plane (h_A and h_B), and the standard deviation (σ) for the isotropic time-averaged Gaussian displacement field. Accordingly, the Hth Fourier component of the W atomic distribution (F_H) can be represented by eq 1.

$$F_H = f_H \exp(2\pi i P_H) = C[c_B \exp(2\pi i \mathbf{H}\cdot\mathbf{r}_B) + c_A \exp(2\pi i \mathbf{H}\cdot\mathbf{r}_A)] \exp(-2\pi^2\sigma^2/d_H^2) \quad (1)$$

where $c_A + c_B = 1$, $r_{A,B}$ are the coordinates of AT and BR sites, and d_H denotes the period of the Hth diffraction plane. In a separate modeling procedure, we considered but found no lateral displacement of W about the AT and BR sites. The least-squares fit to the measured f and P values listed in Table 1 is performed by minimizing the value of $[1/(N_{meas}-N_{para})]\sum_H \sqrt{(f_H^{meas}-f_H^{calcd})^2+(P_H^{meas}-P_H^{calcd})^2}$, where N_{meas} and N_{para} represent the number of measured data and fitting parameters, respectively.

With the best-fit parameters determined as $C = 0.74 \pm 0.07$, $c_B = 0.48 \pm 0.08$, $h_A = 3.28 \pm 0.08$ Å, $h_B = 3.60 \pm 0.08$ Å, and $\sigma = 0.22 \pm 0.04$ Å, the fit results indicate that two symmetrically nonequivalent W sites are occupied with the same occupation fraction, and the bridge site and atop site tungsten atoms locate 0.35 ± 0.08 Å and 0.03 ± 0.08 Å higher than ideal Ti sites, respectively. A similar adsorption geometry was observed for Zn ion adsorption at the aqueous−rutile interface.[26,27]

The refined adsorption geometry of tungsten resembles the structure of WO_2 which has a distorted rutile structure. In the WO_2 bulk structure, the W−O interatomic distance varies from 1.97 to 2.11 Å.[39] Those slightly longer bond lengths than Ti−O distances of rutile TiO_2 (1.95 and 1.98 Å)[40] can explain the higher adsorption height of the bridging tungsten.[41] In our ALD process, relatively small WF_6 molecules were used as the W atom source in which the tungsten is octahedrally coordinated by fluorine. Considering the structural similarities between the rutile TiO_2 substrate and the distorted rutile WO_2, the single-crystal rutile TiO_2(110) substrate provides an optimal bonding geometry for the tungsten to locate at both the atop and bridge sites. The growth of epitaxial oxide thin films that are isostructural to oxide substrates has been observed in many systems.[42,43] By taking an isostructural form with respect to the substrate, ultrathin ALD conformal layers can be highly coherent with the substrate lattice. The XSW analysis study suggests that the ALD process, especially the exchange reaction between surface species and reaction gases, produces conformal layers through replication of underlying atomic-scale structure. This idea is strongly supported by the survival of the (1×1) surface phase, which was observed by LEED following the ALD processing.

The W coverage of 0.38 ML following one ALD cycle implies that 4 of the possible 10.4 oxygen sites (5.2 bridging and 5.2 atop sites) per square nanometer are occupied by W atoms. The surface chemistry for W ALD on SiO_2 exhibits a 2:1 stoichiometry for Si/W.[12] In other words, each W atom deposited during the WF_6 half-reaction replaces two Si atoms from the preceding Si_2H_6 half-reaction. Assuming a similar process for W ALD on TiO_2(110), and if all of the surface oxygen sites (hydroxyl groups) react with Si_2H_6 to form O−SiH_3 surface species, then we expect a W coverage of 0.5 ML. The lower observed coverage of 0.38 ML may result from steric hindrance between the O−SiH_3 surface species that slightly reduces the initial Si coverage. Alternatively, the Si_2H_6 exposures used in this study may not have been sufficient to saturate all of the hydroxyl groups on the TiO_2 surface.

Upon air exposure, the supported W assumes the form of a hydrated tungsten oxide. Indeed, ex situ XPS measurements revealed that the majority of the tungsten has a 6+ oxidation state. Only a minor portion (ca. 10%) of the tungsten exists as W^{4+}, and no metallic tungsten (W^0) was detected. Figure 5 shows XPS spectra from W $4f_{2/7}$, W $4f_{5/2}$, and Ti 3p core levels measured with different photoelectron (PE) takeoff angles (20° and 40°) from the sample surface.

At lower takeoff angles, the relative contribution of the substrate Ti 3p signal is reduced. To resolve the overlapping Ti 3p and W 4f PE peaks, line shape analysis was performed through nonlinear least-squares curve fit of measured spectra to a sum of PEs from substrate (Ti 3p), W^{6+}, and W^{4+}. In the curve fit, the W photoelectrons consist of the $4f_{7/2}$, $4_{f5/2}$ doublets and a satellite peak,[44] and individual PE lines are represented by Voigt functional form (Lorenzian function convoluted with Gaussian function). The spectra taken at two different takeoff angles were fit simultaneously, and the spin−orbit doublet

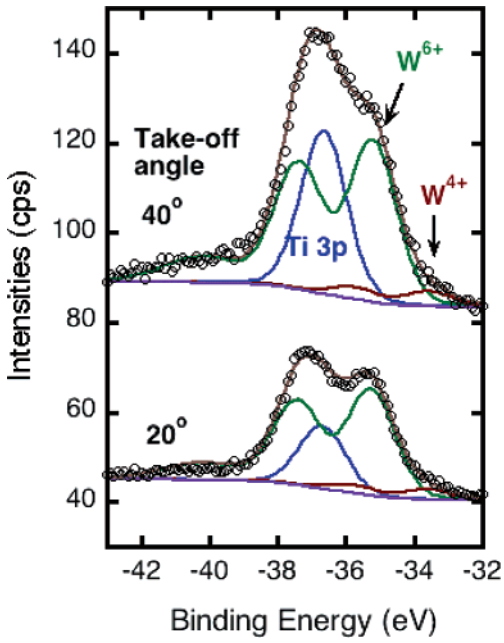

Figure 5. The Ti 3p and W 4f XP spectra measured at two different photoelectron takeoff angles and line shape analysis results. Open circles denote measured photoelectron intensities and spectrum with 40° takeoff angle is vertically shifted for clarity. The spectra were fit with Ti 3p single peak, W $4f_{7/2}$ and $4f_{5/2}$ spin−orbit doublet and satellite peak from W^{6+} and W^{4+} which are represented as solid lines. The following binding energies are obtained as a fit result. Ti 3p at 36.7 eV, W^{6+} $4f_{7/2}$ at 35.3 eV, and W^{4+} $4f_{7/2}$ at 33.6 eV.

separation (−2.18 eV), the area ratio (0.78[45]), and the width ratio (1.0) between W $4f_{7/2}$ and W $4f_{5/2}$ were fixed during the fitting procedure. Minor charging was observed, and the binding energies were corrected on the basis of the binding energy of Ti $2p_{3/2}$ from TiO_2(110) at 458.5 eV.[46] The binding energies are positioned at 36.7 eV for Ti 3p, 35.3 eV for W^{6+} $4f_{7/2}$, and 33.6 eV for W^{4+} $4f_{7/2}$. The observed binding energies are similar to those obtained from supported tungsten oxides prepared on TiO_2 powders for Ti 3p at 36.9 and 37.3 eV, W^{6+} $4f_{7/2}$ at 35.1 and 35.5 eV, and W^{4+} $4f_{7/2}$ at 33.3 eV.[44,47]

From previous studies of the ALD process using WF_6 and B_2H_6, 3×10^{-3} atom % residual F was found in a multilayer film.[48] On the basis of our XPS, we found that most of the fluorine was removed from surfaces after air exposure. We prepared and studied several different samples and found variations in the amount of residual F. However, the XSW measured f_H and P_H values did not vary.

Mixtures of anatase and rutile powders have been used as supports in previous studies of supported tungsten oxide. On the basis of XANES and EXAFS measurements, it was claimed that dehydrated tungsten oxide prepared by impregnation consists primarily of tetrahedrally coordinated tungsten.[49] The appearance of tungsten in octahedral sites was observed at high coverage. However, in hydrated tungsten oxides, only octahedrally coordinated tungsten was observed.[49] Raman spectroscopy results were interpreted in terms of a hydrated WO_x film with tetrahedrally and octahedrally coordinated tungsten atoms that are converted to a surface species with octahedrally coordinated tungsten upon dehydration.[50]

Despite these contradictory conclusions, similar structural models were proposed for dehydrated tungsten oxides. Those models have proposed surface WO_x structure as a mixture of tetrahedrally coordinated WO_4 and octahedrally coordinated WO_5 [49] and a distorted WO_6 octahedron,[50] respectively. Common to both proposed models is that only the atop site tungsten

has been considered. No structural model was proposed for the hydrated tungsten oxide. Our current study clearly indicates the existence of bridge site tungsten in a hydrated oxide form. It requires further studies to correlate the adsorption geometry to the local structures deduced from catalysts supported on powder substrates.

Conclusions

This is the first atomic-scale structural determination of a supported catalytic phase under ambient conditions. The results suggest that monolayer dispersion of supported oxides can be achieved when the cations locate as if they were the next layer in the bulk structure of the supporting oxide. The study opens a possibility that the ALD method for supported catalyst material preparation could provide a bridge over the "materials preparation gap" that typically separates practical, high-surface-area catalytic materials from single-crystal model catalytic materials.

Acknowledgment. The authors thank the XOR-BESSRC staff and Zhan Zhang for technical assistance. This work was supported by the DOE under contract no. DE-FG02-03ER15457 to the Institute for Environmental Catalysis at Northwestern University. Use of the Advanced Photon Source was supported by the U.S. Department of Energy, Office of Science, Office of Basic Energy Sciences, under contract no. W-31-109-ENG-38. The work made use of Northwestern University Central Facilities supported by the MRSEC program of the NSF (DMR-0520513).

References and Notes

(1) Wachs, I. E. *Catal. Today* **2005**, *100*, 79.
(2) Kingon, A. I.; Maria, J. P.; Streiffer, S. K. *Nature (London)* **2000**, *406*, 1032.
(3) Shi, D. *Functional thin films and functional materials: new concepts and technologies*; Springer: Berlin, 2003.
(4) Hagleitner, C.; Hierlemann, A.; Lange, D.; Kummer, A.; Kerness, N.; Brand, O.; Baltes, H. *Nature (London)* **2001**, *414*, 293.
(5) Yeh, W. K.; Chen, M. C.; Wang, P. J.; Liu, L. M.; Lin, M. S. *Thin Solid Films* **1995**, *270*, 462.
(6) Hand, A. *Semicond. Int.* **2003**, *26* (May), 46.
(7) Elam, J. W.; Routkevitch, D.; Mardilovich, P. P.; George, S. M. *Chem. Mater.* **2003**, *15*, 3507.
(8) Pellin, M. J.; Stair, P. C.; Xiong, G.; Elam, J. W.; Birrell, J.; Curtiss, L.; George, S. M.; Han, C. Y.; Iton, L.; Kung, H.; Kung, M.; Wang, H. H. *Catal. Lett.* **2005**, *102*, 127.
(9) King, J. S.; Heineman, D.; Graugnard, E.; Summers, C. *J. Appl. Surf. Sci.* **2005**, *244*, 511.
(10) Ihanus, J.; Hanninen, T.; Hatanpaa, T.; Aaltonen, T.; Mutikainen, I.; Sajavaara, T.; Keinonen, J.; Ritala, M.; Leskela, M. *Chem. Mater.* **2002**, *14*, 1937.
(11) Houssa, M. *High-K gate dielectrics*; Series in Materials Science and Engineering; Institute of Physics: Bristol, UK, 2003.
(12) Elam, J. W.; Nelson, C. E.; Grubbs, R. K.; George, S. M. *Surf. Sci.* **2001**, *479*, 121.
(13) Elam, J. W.; Nelson, C. E.; Grubbs, R. K.; George, S. M. *Thin Solid Films* **2001**, *386*, 41.
(14) Klaus, J. W.; Ferro, S. J.; George, S. M. *Thin Solid Films* **2000**, *360*, 145.
(15) Lakomaa, E. L. *Appl. Surf. Sci.* **1994**, *75*, 185.
(16) Suntola, T.; Simpson, M. *Atomic layer epitaxy*; Blackie: Glasgow, 1990.
(17) Sechrist, Z. A.; Fabreguette, F. H.; Heintz, O.; Phung, T. M.; Johnson, D. C.; George, S. M. *Chem. Mater.* **2005**, *17*, 3475.
(18) Dulub, O.; Hebenstreit, W.; Diebold, U. *Phys. Rev. Lett.* **2000**, *84*, 3646.
(19) Tauster, S. J.; Fung, S. C.; Garten, R. L. *J. Am. Chem. Soc.* **1978**, *100*, 170.
(20) Batterman, B. W. *Phys. Rev. Lett.* **1969**, *22*, 703.
(21) Cheng, L.; Fenter, P.; Bedzyk, M. J.; Sturchio, N. C. *Phys. Rev. Lett.* **2003**, *90*, 255503.
(22) Golovchenko, J. A.; Patel, J. R.; Kaplan, D. R.; Cowan, P. L.; Bedzyk, M. *J. Phys. Rev. Lett.* **1982**, *49*, 560.
(23) Zegenhagen, J. *Surf. Sci. Rep.* **1993**, *18*, 199.
(24) Escuadro, A. A.; Goodner, D. M.; Okasinski, J. S.; Bedzyk, M. J. *Phys. Rev. B* **2004**, 70, 235416.
(25) Okasinski, J. S.; Kim, C.-Y.; Walko, D. A.; Bedzyk, M. J. *Phys. Rev. B* **2004**, *69*, 041401.
(26) Zhang, Z.; Fenter, P.; Cheng, L.; Sturchio, N. C.; Bedzyk, M. J.; Machesky, M. L.; Wesolowski, D. J. *Surf. Sci.* **2004**, *554*, L95.
(27) Zhang, Z.; Fenter, P.; Cheng, L.; Sturchio, N. C.; Bedzyk, M. J.; Predota, M.; Bandura, A.; Kubicki, J. D.; Lvov, S. N.; Cummings, P. T.; Chialvo, A. A.; Ridley, M. K.; Benezeth, P.; Anovitz, L.; Palmer, D. A.; Machesky, M. L.; Wesolowski, D. J. *Langmuir* **2004**, *20*, 4954.
(28) Bedzyk, M. J.; Cheng, L. W. *Rev. Mineral. Geochem.* **2002**, *49*, 221.
(29) Fenter, P.; Cheng, L.; Rihs, S.; Machesky, M.; Bedzyk, M. J.; Sturchio, N. C. *J. Colloid Interface Sci.* **2000**, *225*, 154.
(30) Gupta, J.; Sudijono, J.; Hsia, L. C.; Singh, S.; Tat, T. W. 90 nm contact fill performance using ALD-W as nucleation layer; In proceedings of the Advanced Metallization Conference 2003 (AMC 2003); Warrendale, Materials Research Society.
(31) Granqvist, C. G. *Handbook of inorganic electrochromic materials*; Elsevier: Amsterdam, 1995.
(32) Soled, S. L.; Mcvicker, G. B.; Murrell, L. L.; Sherman, L. G.; Dispenziere, N. C.; Hsu, S. L.; Waldman, D. *J. Catal.* **1988**, *111*, 286.
(33) Diebold, U. *Appl. Phys. A* **2003**, *76*, 681.
(34) Kurtz, R. L.; Stock-Bauer, R.; Msdey, T. E.; Roman, E.; De Segovia, J. *Surf. Sci.* **1989**, *218*, 178.
(35) Lindan, P. J. D.; Harrison, N. M.; Holender, J. M.; Gillan, M. J. *Chem. Phys. Lett.* **1996**, *261*, 246.
(36) Lindan, P. J. D.; Harrison, N. M.; Gillan, M. J. *Phys. Rev. Lett.* **1998**, *80*, 762.
(37) Epling, W. S.; Peden, C. H. F.; Henderson, M. A.; Diebold, U. *Surf. Sci.* **1998**, *413*, 333.
(38) Elam, J. W.; Groner, M. D.; George, S. M. *Rev. Sci. Instrum.* **2002**, *73*, 2981.
(39) Palmer, D. J.; Dickens, P. G. *Acta Crystallogr., B* **1979**, *35*, 2199.
(40) Grant, F. A. *Rev. Mod. Phys.* **1959**, *31*, 646.
(41) Simple geometric consideration based on W−O bond length and unperturbed underlying oxygen atoms gives higher bridge site than atop site when the W−O bond length exceeds 1.89 Å.
(42) Chambers, S. A. *Surf. Sci. Rep.* **2000**, *39*, 105.
(43) Surnev, S.; Ramsey, M. G.; Netzer, F. P. *Prog. Surf. Sci.* **2003**, *73*, 117.
(44) Fiedor, J. N.; Proctor, A.; Houalla, M.; Hercules, D. M. *Surf. Interface Anal.* **1995**, *23*, 204.
(45) Scofield, J. H. *J. Electron Spectrosc. Relat. Phenom.* **1976**, *8*, 129.
(46) Gopel, W.; Anderson, J. A.; Frankel, D.; Jaehnig, M.; Phillips, K.; Schafer, J. A.; Rocker, G. *Surf. Sci.* **1984**, *139*, 333.
(47) Scholz, A.; Schnyder, B.; Wokaun, A. *J. Mol. Catal., A* **1999**, *138*, 249.
(48) Yang, M.; Chung, H.; Yoon, A.; Fang, H.; Zhang, A.; Knepfler, C.; Jackson, R.; Byun, J. S.; Mak, A.; Eizenberg, M.; Xi, M.; Kori, M.; Sinha, A. K. Atomic layer deposition of tungsten film from $WF_6B_2H_6$: nucleation layer for advanced semiconductor devices; In *Proceedings of the Advanced Metallization Conference 2001 (AMC 2001)*; Warrendale, Materials Research Society.
(49) Hilbrig, F.; Gobel, H. E.; Knozinger, H.; Schmelz, H.; Lengeler, B. *J. Phys. Chem.* **1991**, *95*, 6973.
(50) Vuurman, M. A.; Wachs, I. E.; Hirt, A. M. *J. Phys. Chem.* **1991**, *95*, 9928.